Investigation of gear walk suppression while maintaining braking performance in a main landing gear

Qiaozhi Yin[a,b], Jason Zheng Jiang[b], Simon A. Neild[b], Hong Nie[a,*]

[a]State Key Laboratory of Mechanics and Control of Mechanical Structures, Nanjing University of Aeronautics and Astronautics, Nanjing 210016, China

[b]Department of Mechanical Engineering, University of Bristol, Bristol BS8 1TR, UK

*Corresponding author. Nanjing University of Aeronautics and Astronautics, Nanjing 210016, China. Tel.: +86 25 8489 1024.

E-mail addresses: yinqiaozhi@nuaa.edu.cn (Q.Z.Yin), z.jiang@bristol.ac.uk (J.Z.Jiang), simon.neild@bristol.ac.uk (S.A.Neild), hnie@nuaa.edu.cn (H.Nie).

Abstract: In this paper, a nonlinear dynamic landing gear model considering the influence of the coupling of the shock absorber stroke variation and the landing gear longitudinal motion with an anti-skid PID braking control system that captures gear walk is established. This gear walk model is verified by comparing with the response from a virtual prototype model. Then a parameter sensitivity analysis is carried out to find out the parameters with greater effects on gear walk and braking performance. The short time Fourier transform is employed to study the transient gear walk amplitude-frequency response, whose results are used to define the optimization constraints. A feedforward controller is proposed as part of the braking control law. Single-objective optimizations are then carried out to improve the gear walk performance while maintaining the braking efficiency. It is shown that the feedforward control, together with the PID feedback controller, can provide 25.68% reduction of the maximum gear walk angle while satisfying other constraints. The stability and robustness of the optimized braking law is verified under different working conditions. Multi-objective optimization is then used to highlight the trade-off between the gear walk vibration and the braking efficiency.

Keywords: gear walk, braking, short time Fourier transform, design of experiment, optimization

1. Introduction

Brake-induced vibrations result from different types of frictions in braking systems and usually lead to detrimental vibrations, noise and excessive wear [1]. One form of aircraft brake vibration is the low-frequency brake-induced vibration, called gear walk. It is defined as the longitudinal fore and aft motion of the landing gear, caused by the varying ground friction force and the braking torque during the braking process. Gear walk can build up to various levels, creating passenger discomfort, structural failures of landing gear components and even cause severe accidents [2]. Both the landing gear structure and the braking control system influence the gear walk phenomenon [3]. Therefore, it is important to include both in a gear walk dynamic model. The possibility of reducing deleterious vibrations while achieving improved braking efficiency through parameter selection is a key design trade-off. This is the focus of the present study. The problem is complicated due to the interactions between the landing gear, wheel, brakes and anti-skid braking system [4].

On the aspect of gear walk modeling, Zhang and Zhu [5] built a gear walk dynamic model considering the landing gear shock absorber as a spring-damper system without mass. Karthik and Kambiz [6] established a lumped-parameter model of the landing gear with a rigid strut, a braking wheel and a spring system connecting the landing gear to the fuselage. Khapane [7] built a gear walk model in a dynamic software and implemented two different braking control laws. Using this it was verified that the anti-skid algorithm is effective in terms of mitigating gear vibrations and maintaining stability. Lernbeiss and Plochl [8] focused on eigen-frequency analysis of the shock strut during taxiing process and concluded that gear walk would affect the braking process. Gualdi et al. [9] applied the multidisciplinary multibody modeling method to analyze gear walk vibration characteristics under different operational conditions. Comparing to the previous works regarding gear walk modeling, the influence of the coupling of the shock absorber stroke variation and the landing gear longitudinal motion on the main wheel slip rate and gear walk vibration is added in the dynamic model in this study.

Regarding the gear walk mitigation for landing gears, studies have shown that it is necessary to use models including both the landing gear dynamic model and the braking control system [10]. The genetic algorithm (GA), which is applied to optimize the key parameters in the control strategy of electric vehicle electro-hydraulic composite braking system [11], has been shown to be effective to obtain the optimal anti-skid braking control parameters in this paper. In addition, after successful sensitivity analysis of landing gear structure parameters in [9], the analysis is extended to carry out both the structural and the braking control parameters together to investigate their influence on gear walk in this study. Also, a multi-objective optimization [12] technique has been employed effectively here to optimize the vibration performance while maintaining the braking efficiency at the same time. Anti-skid braking control laws based on the optimal slip rate [13]-[14] can result in a significant overshoot of the braking torque as the braking control system is initiated [15]. It has also been shown that both smoothing the braking control signal and decreasing the overshoot of the braking torque are capable to reduce the low-frequency brake-induced vibration [16]. Therefore, a feedforward controller is proposed as part of the braking control law here to improve the performance.

The purpose of this study is to reduce the gear walk vibrations while maintaining the braking efficiency. In Section 2, a nonlinear dynamic gear walk model including both the landing gear structure and the braking control system is established. The influence of the anti-skid PID braking control system on gear walk is taken into consideration when calculating the actual slip rate. Then the response is compared with an industrially verified virtual prototype model. In Section 3, the performance criteria are defined. In order to fully characterize the gear walk response, performance criteria based on both the time domain response [17]-[18] and the frequency domain response are then proposed. The short-time Fourier transform method [19] is used to capture the transient vibration performance and the frequency relationship between the excitation braking torque and the response gear walk angle is found out. Then in Section 4, the parameter sensitivity is analyzed via the Optimal Latin Hypercube Design method [20]. In Section 5, single-objective optimizations are firstly carried out with significant improvement of gear walk performance obtained and the robustness of the optimized control system is verified under different working conditions. Then the Pareto optimal solution set [21] is obtained via multi-objective optimization. This allows the trade-off between the braking efficiency and vibration suppression performance to be demonstrated. Conclusions are drawn in Section 6.

2 Gear walk system modeling

2.1 Gear walk dynamic model

Figure 1 shows the schematic diagram of the gear walk dynamic model including the equivalent mass of the fuselage, the braking wheel, as well as the landing gear strut consisting of an outer cylinder and a piston rod. The torsional spring-damper system, with coefficients k_λ, c_λ representing the landing gear strut longitudinal stiffness and damping, connects the fuselage and the landing gear. λ is the gear walk angle between the vertical y_f coordinate axis and the landing gear strut center line, indicating the vibration amplitude. The shock absorber is also simplified as a spring-damper system with parameters k_s, c_s. The relative movement between the outer cylinder and the piston rod is restrained only in the axial direction and the shock absorber stroke is *s*. The braking wheel is composed of a rolling hub and tire travelling in the x_w direction. It is assembled on the landing gear strut and rotates around the wheel axle. In order to study the influence of the tire longitudinal property on gear walk, similar to [22], the tire is connected to the wheel hub by a linear spring k_{tx} and a dashpot c_{tx} representing the elastic and damping characteristics of the tire. Also, the tire is assumed to have a linear spring characteristic k_t in the vertical direction [23].

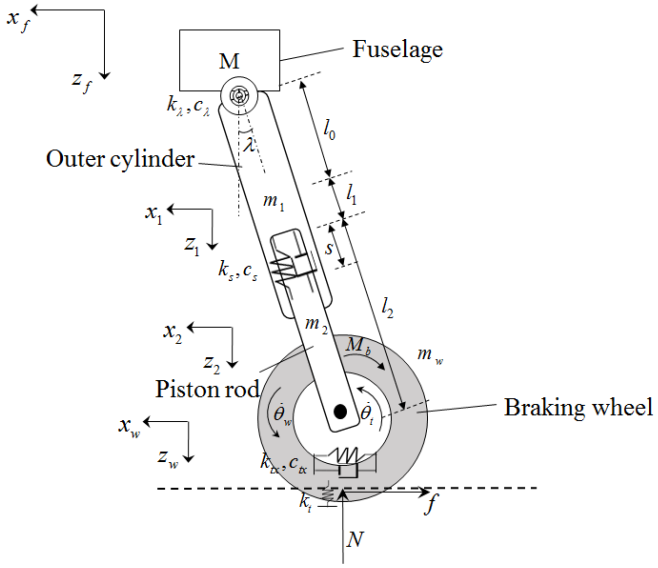

Fig. 1. The schematic diagram of gear walk dynamics model

The gear walk dynamic model is established using the Lagrange's equation [24]. The specific formulas of every term in the Lagrange's equation (See Eq. (A.1)-(A.6)), and the kinematic relationships (See Eq. (A.7)-(A.12)) for the gear walk model are all shown in Appendix A.

In the gear walk dynamic system, the fuselage has two degrees of freedom (DOFs), the forward and the vertical motion x_f and z_f respectively. The outer cylinder and the piston rod both have three DOFs including x_1, z_1 (for the former), x_2, z_2 (for the later) and rotation about the attachment between the landing gear and the fuselage λ (for both). The wheel hub and the tire both have four DOFs including x_w, z_w, λ (for both) and the rotation angles about the wheel axle θ_w (for the former) and θ_t (for the later), respectively.

Even though every part in the model has several DOFs, the constraints and the geometric

relationships between the parts reduce the whole gear walk model to a six-DOF model using generalized coordinates

$$q_i = [x_f, z_f, \lambda, \theta_w, s, \theta_t] \quad (i = 1, 2, \ldots, 6). \tag{1}$$

The tire vertical deflection results from the ground reaction force and is related to coupling of the vertical displacement of the fuselage, the gear walk angle and the shock absorber stroke, using

$$\delta_t = z_f - s \cdot \cos\lambda + (l_0 + l_1 + l_2)(\cos\lambda - 1), \tag{2}$$

where δ_t is the tire vertical deflection. l_0 is the distance between the landing gear strut top and the outer cylinder mass center. l_1 is the distance between the top of the piston rod and the outer cylinder mass center when the shock absorber is at the original place. l_2 is the length of the piston rod.

The rolling radius R_g is defined as the difference of the original braking tire radius R_w and the tire deflection, giving

$$R_g = R_w - \delta_t = R_w - z_f + s \cdot \cos\lambda - (l_0 + l_1 + l_2)(\cos\lambda - 1). \tag{3}$$

The equations of motion are derived using Eqs. (A.7)-(A.12). The kinematic relation equations are substituted into the Lagrange's energy terms and six dynamic equations of the gear walk dynamics model corresponding to the six generalized coordinates are obtained, which can be written as

$$\begin{aligned}&(M + m_1 + m_2 + m_w)\ddot{x}_f - [m_1 l_0 + m_2(l_0 + l_1 - s + l_2/2) + m_w(l_0 + l_1 - s + l_2)] \cdot \\ &(\ddot{\lambda}\cos\lambda - \dot{\lambda}^2 \sin\lambda) + 2(m_2 + m_w)\dot{s} \cdot \dot{\lambda}\cos\lambda + (m_2 + m_w)\ddot{s} \cdot \sin\lambda \\ &= -\mu_x k_t [z_f - s\cos\lambda + (l_0 + l_1 + l_2)(\cos\lambda - 1)],\end{aligned} \tag{4}$$

$$\begin{aligned}&(M + m_1 + m_2 + m_w)\ddot{z}_f - [m_1 l_0 + m_2(l_0 + l_1 - s + l_2/2) + m_w(l_0 + l_1 - s + l_2)] \cdot \\ &(\ddot{\lambda}\sin\lambda + \dot{\lambda}^2 \cos\lambda) + 2(m_2 + m_w)\dot{s} \cdot \dot{\lambda}\sin\lambda - (m_2 + m_w)\ddot{s} \cdot \cos\lambda \\ &= (M + m_1 + m_2 + m_w)g - k_t(z_f - s\cos\lambda + (l_0 + l_1 + l_2)(\cos\lambda - 1)),\end{aligned} \tag{5}$$

$$\begin{aligned}&[J_1 + J_2 + J_{w\lambda} + 2m_1 l_0^2 + 2m_2(l_0 + l_1 - s + l_2/2)^2 + 2m_w(l_0 + l_1 - s + l_2)^2]\ddot{\lambda} + c_\lambda \dot{\lambda} + k_\lambda \lambda \\ &-[m_1 l_0 + m_2(l_0 + l_1 - s + l_2/2) + m_w(l_0 + l_1 - s + l_2)](\ddot{x}_f \cos\lambda + \ddot{z}_f \sin\lambda) \\ &-2[m_2(l_0 + l_1 - s + l_2/2) + m_w(l_0 + l_1 - s + l_2)] \cdot \dot{\lambda} \cdot \dot{s} \\ &= -[m_1 l_0 + m_2(l_0 + l_1 - s + l_2/2) + m_w(l_0 + l_1 - s + l_2)]g \sin\lambda \\ &+k_t[z_f - s\cos\lambda + (l_0 + l_1 + l_2)(\cos\lambda - 1)](l_0 + l_1 - s + l_2)\sin\lambda \\ &+\mu_x k_t[z_f - s\cos\lambda + (l_0 + l_1 + l_2)(\cos\lambda - 1)](l_0 + l_1 - s + l_2)\cos\lambda,\end{aligned} \tag{6}$$

$$J_w \ddot{\theta}_w + k_{tx} \cdot R_h^2 \cdot (\theta_w - \theta_t) + c_{tx} \cdot R_h^2 \cdot (\dot{\theta}_w - \dot{\theta}_t) = 0, \tag{7}$$

$$\begin{aligned}&(m_2 + m_w)(\ddot{s} + \ddot{x}_f \sin\lambda - \ddot{z}_f \cos\lambda) + c_s \dot{s} + k_s s + [m_2(l_0 + l_1 - s + l_2/2) + m_w(l_0 + l_1 - s + l_2)]\dot{\lambda}^2 \\ &= -(m_2 + m_w)g\cos\lambda + k_t \cos\lambda[z_f - s\cos\lambda + (l_0 + l_1 + l_2)(\cos\lambda - 1)] \\ &-\mu_x k_t(z_f - s\cos\lambda + (l_0 + l_1 + l_2)(\cos\lambda - 1))\sin\lambda,\end{aligned} \tag{8}$$

$$\begin{aligned}&J_t \ddot{\theta}_t + k_{tx} \cdot R_h^2 \cdot (\theta_t - \theta_w) + c_{tx} \cdot R_h^2 \cdot (\dot{\theta}_t - \dot{\theta}_w) \\ &= \mu_x k_t(z_f - s\cos\lambda + (l_0 + l_1 + l_2)(\cos\lambda - 1)) \cdot (R_w - z_f + s\cos\lambda - (l_0 + l_1 + l_2)(\cos\lambda - 1)) - M_b.\end{aligned} \tag{9}$$

Here M is the equivalent mass of the fuselage, m_1, m_2, m_w are the masses of the outer cylinder, the piston rod and the braking wheel, respectively. g is the gravitational acceleration. J_1, J_2, J_{wt} are the rotational inertias of the outer cylinder, the piston rod and the braking wheel about their own mass centers, respectively. J_w, J_t are the rotational inertias about the braking wheel axle of the wheel hub and the tire. R_h is the radius of the wheel hub. μ_x is the friction coefficient between the ground and the tire, and M_b is the braking torque on the wheel.

2.2 Anti-skid braking system model

Gear walk is a type of low-frequency brake-induced vibration caused by the varying braking torque controlled by the anti-skid braking control system. Therefore, the braking control system has great impact on the gear walk performance. Figure 2 illustrates the operating principle of the anti-skid braking system.

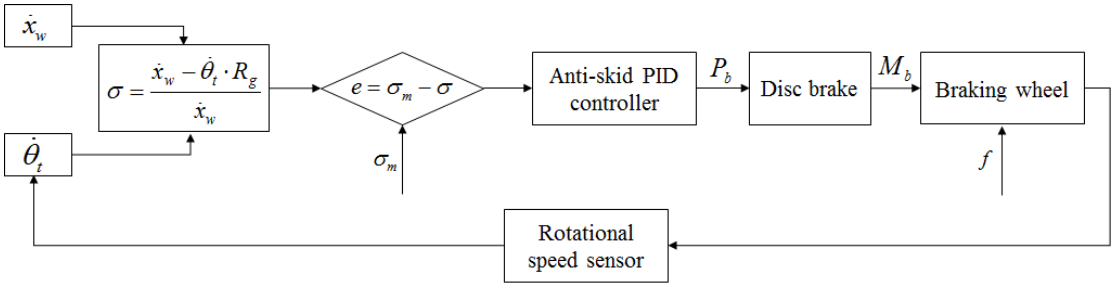

Fig. 2. Anti-skid braking control system principle diagram

The input of the anti-skid PID controller is the difference e between the optimal slip rate σ_m and the actual slip rate σ. Since the fore-aft motion of the landing gear resulting from gear walk leads to different velocities of the fuselage and the braking wheel, the actual slip rate should be calculated using $\dot{x}_w$ rather than $\dot{x}_f$ in the traditional expression [25] to avoid the inappropriate braking torque caused by the inaccurate actual slip rate. Thus the actual slip rate is defined as

$$\sigma = \frac{\dot{x}_w - \dot{\theta}_t \cdot R_g}{\dot{x}_w}. \tag{10}$$

The ground friction coefficient μ_x [26] is dependent mainly on the slip rate and the nonlinear relationship between μ_x and σ is

$$\begin{aligned} \mu_x &= 0.8\sin(1.5344 \times \arctan(14.0326\sigma)) \quad \text{Dry runway,} \\ \mu_x &= 0.4\sin(2.0192 \times \arctan(8.2098\sigma)) \quad \text{Wet runway,} \\ \mu_x &= 0.2\sin(2.0875 \times \arctan(7.201788\sigma)) \quad \text{Icy runway.} \end{aligned} \tag{11}$$

From Eq. (11), it can be seen that the ground friction coefficient reaches the maximum value when the slip rate is about 0.15 corresponding to the optimal slip rate. So the braking control system tries to control the actual slip rate to approach the optimal slip rate, aiming to improve the braking efficiency. The braking torque and the ground friction force on the tire make the braking wheel rotate and a speed sensor transmits the braking wheel rotational velocity to the controller to calculate the slip rate, constituting a closed-loop braking control system.

The output of the PID controller is the braking pressure P_b acting on the brake mechanism and the relative rotational motion of the brake rotors and the stators transfer the braking pressure to the

braking torque M_b. In order to pull apart the braking rotors and the stators after the braking pressure is released, a return spring is fixed between the braking pads. Therefore, when the braking pressure is smaller than P_0, the braking torque is 0 due to the return spring force. Moreover, due to the wear and elastic deformation of the braking pads, the static moment characteristic curve is a hysteresis loop with a dead band. Based on these observations, the experimental formulas [27] of braking torque and braking pressure is

$$M_b = \begin{cases} 0 & P_b < P_0 \\ k_2 \cdot (P_b - P_0) & P_0 \le P_b \le \dfrac{M_1}{k_2} + P_0 \\ M_1 & \dfrac{M_1}{k_2} + P_0 \le P_b \le rP, \\ M_1 & P_0 \le P_b \le \dfrac{M_1}{k_1} + P_0 \\ k_1 \cdot (P_b - P_0) & \dfrac{M_1}{k_1} + P_0 \le P_b \le P_m \end{cases} \tag{12}$$

$$k_1 = \frac{M_{sm}}{P_m - P_0}, \tag{13}$$

$$k_2 = \frac{M_{sm}}{P_x - P_0}, \tag{14}$$

where P_0 is the braking pressure loss due to the space between the braking pads, M_1 is the braking torque of the last moment, rP is the braking pressure of the last moment, M_{sm} is the maximum value of the braking torque, P_m is the maximum value of the braking pressure, P_x is the maximum value of the hysteresis pressure.

2.3 Model verification

The dynamic gear walk model and the anti-skid braking control system introduced in Sub-Section 2.1&2.2 are built in MATALB. The landing working condition is that the runway surface is dry and smooth. The landing forward velocity is 77m/s. The landing gear initial vertical sink speed is 0.5m/s. Table 1 shows the original parameters of the gear walk model including the key structural parameters and the braking control parameters. K_P, K_I, K_D are the three PID controller parameters in the anti-skid braking system. Other parameters and their values used in the model are illustrated in Appendix B.

Table 1

Key parameters and their values used in the gear walk model

(a) Structure parameters

Structure Parameter	k_λ ($\mathrm{N \cdot m/rad}$)	c_λ ($\mathrm{N \cdot m \cdot s/rad}$)	k_{tx} ($\mathrm{N/m}$)	c_{tx} ($\mathrm{N \cdot s/m}$)
Value (Default)	1746000	13800	1492000	1980

(b) Control parameters

Control Parameter	K_P	K_I	K_D	P_0 (MPa)	P_x (MPa)

Value (Default)	105	2000	1	1	8.3

In a previous study, a virtual prototype model [28] including the tire nonlinearity in a multibody dynamics software LMS Vitrual.Lab Motion was built and verified via the landing gear drop tests. Owing to the fact that the structural parameters are difficult to change during the sensitivity analysis and the optimization process, and also in order to improve the optimization efficiency greatly without spending a lot of time on transmitting the data between two softwares when conducting the co-simulation, the mathematical model in MATLAB/Simulink is built to replace the multibody one. Here the multibody model is used to verify the validity of the mathematical model. Figure 3 illustrates the gear walk virtual prototype model in LMS Vitrual.Lab Motion. The structural and control parameters are the same as those in the mathematical model shown in Table 1.

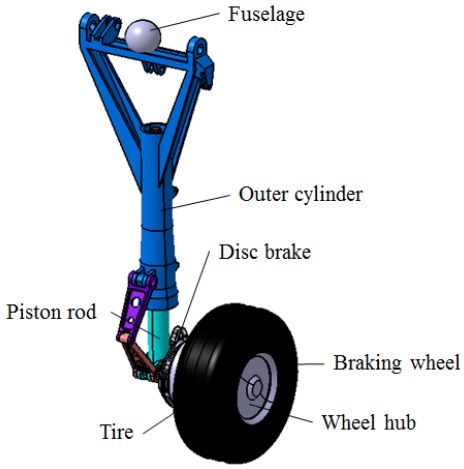

Fig. 3. Gear walk virtual prototype modeling

Figure 4 demonstrates the simulation results of the mathematical model with original parameters and Table 2 shows the comparison results of the mathematical model and virtual test prototype model. From Figure 4(a) and Table 2, it can be seen that the difference of the two results of the aircraft braking distance is only 1.10%. In Figure 4(b), the slip rate equals 1 since the braking wheel is stationary at the moment the tire touches the ground. The tire accelerates to the aircraft velocity and rotates without slipping before the braking control system starts to work from 1s. Immediately after the braking is first applied, the slip rate peaks due to the large braking torque with a rate of 0.83 and 0.91 for the mathematical and virtual test prototype model respectively. Figures 4(c) and 4(d) show the gear walk angle response representing the fore and aft motion of the landing gear strut and the braking torque acting on the brake mechanism. The difference of the maximum gear walk angle is approximately 3.90%. The trend of the variation for the braking torque is almost the same as the gear walk angle.

The mathematical gear walk model in MATALB/Simulink is established with lumped mass of every component, while the virtual prototype model is multi-rigid-body system with distributed mass. Therefore, the simulation results between the two models are not exactly the same, but the differences are all within 10% and the trends of the curves agree well with each other, verifying that the mathematical gear walk model is correct and effective.

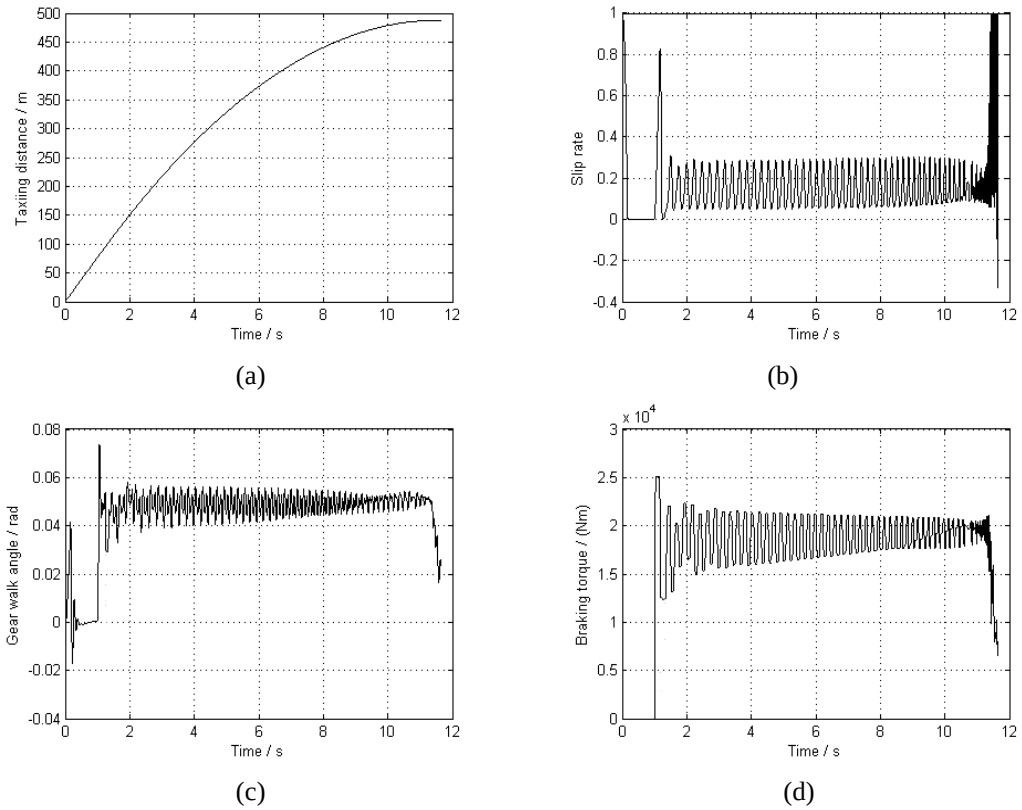

Fig. 4. Simulation results of mathematical model with original parameters. (a) Taxiing distance; (b) slip rate; (c) gear walk angle; (d) braking torque.

Table 2

Comparison of mathematical model and virtual test prototype model simulation results

	Taxiing distance (m)	Maximum slip rate	Maximum gear walk angle (rad)	Maximum braking torque (Nm)
Mathematical model	488.4	0.83	0.074	25100
Virtual test prototype	483.1	0.91	0.077	25100
Error (%)	+1.10%	-8.79%	-3.90%	0

3 Performance criteria

3.1 Performance definition

While applying the brakes can trigger gear walk vibration, they are crucial for ensuring a reasonable taxiing distance. Therefore, the taxiing distance, x_f , is included as a performance measure. Figure 5 demonstrates the other definitions of gear walk angle and braking torque responses. The peak magnitude $\lambda_{\max}$ shown in Figure 5(a) is defined by the maximum gear walk angle during the braking process. In addition, the vibration attenuation of gear walk is another vital indicator to evaluate the vibration system performance. Hence A_λ representing the rest maximum gear walk angle amplitude following the first peak $\lambda_{\max}$ during the whole braking process is considered as one performance measure as well. Also, since gear walk is a transient behavior and the vibration arises from the alternating braking force excitation, the frequencies of the braking

torque and the gear walk are both complicated and changing in the whole time domain and high frequency braking operation and vibration will both damage the landing gear structure and the brake mechanism. Thus only taking $\lambda_{\max}$ and A_{λ} as the design specifications to measure the gear walk system is not enough. From Figure 5(a), it can be seen that the gear walk angle may fluctuate seriously under high frequency. So the high-frequency amplitudes also need to be controlled when trying to improve the vibration performance. Here $A_{\lambda(f_{\lambda}\geq 10\,\mathrm{Hz})}$ represents the gear walk angle amplitudes when the gear walk angle vibration frequency is above 10Hz and this value is also regarded as one of the performance criteria to evaluate the vibration characteristics. Furthermore, although gear walk is a kind of forced vibration and the frequency components of the gear walk angle and the braking torque are the same, it is insufficient to just control the gear walk response. Therefore, similar to $A_{\lambda(f_{\lambda}\geq 10\,\mathrm{Hz})}$, $A_{Mb(f_{Mb}\geq 10\,\mathrm{Hz})}$ is defined as another assessment index to denote the braking torque amplitude when the braking frequency is above 10Hz in Figure 5(b).

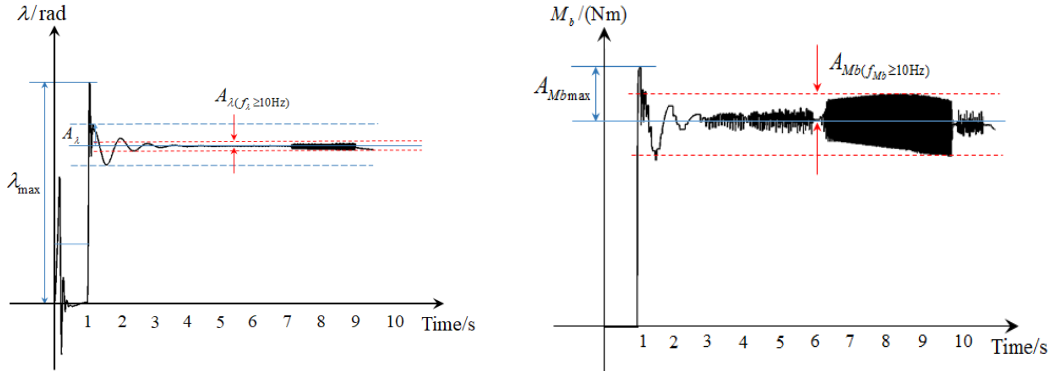

(a) (b)

Fig. 5. The definitions of gear walk system response during DOE process. (a) Gear walk angle; (b) Braking torque.

3.2 Performance assessments obtained by time and frequency domain simulation

Among these five outputs, x_f and $\lambda_{\max}$ can be obtained from the time-domain simulation results shown in Figure 4, while A_{λ}, $A_{\lambda(f_{\lambda}\geq 10\,\mathrm{Hz})}$ and $A_{Mb(f_{Mb}\geq 10\,\mathrm{Hz})}$ need to be calculated based on the amplitude-frequency response. We will show in this sub-section that the values of A_{λ}, $A_{\lambda(f_{\lambda}\geq 10\,\mathrm{Hz})}$ and $A_{Mb(f_{Mb}\geq 10\,\mathrm{Hz})}$ can all be obtained by the Short Time Fourier Transform (STFT) method. This enables more accurate transient response in the parameter sensitivity analysis and optimization process.

Figure 6 illustrates the amplitude-frequency curves of gear walk response with original parameters. Since gear walk is a transient-state behavior, the STFT method is applied to characterize the amplitude-frequency performance of the gear walk angle and the braking torque in the whole time domain. The results are presented in Figures 6(a) and 6(b) respectively. The spectrograms with a top view are obtained by the Fourier spectrogram command `spectrogram` in MATLAB. A 512 points Hamming window is used with an overlap between sections of 256 sample points. The number of the sampling points to calculate the discrete Fourier transform is the default value of this command and the sampling frequency is 1000 Hz. As the frequency content varies significantly with time, these spectrograms are used to define the objectives and the constraints during the optimization process. From Figure 6(a), we can see that the gear walk vibration frequency response is almost entirely under 15Hz and as times goes by, the frequency decreases. The stable gear walk

angle offset is about 0.09rad and the maximum amplitude is larger than 0.012rad, taking place when the braking control system starts to work at 1s. Figure 6(b) shows that the braking torque frequency is mainly within a boundary of 3Hz-8Hz and only reaches the peak during the first 0.5s of braking process. The braking torque maximum amplitude is larger than 4000N before 2s and smaller than 3000N comprised of two main amplitude components after 2s.

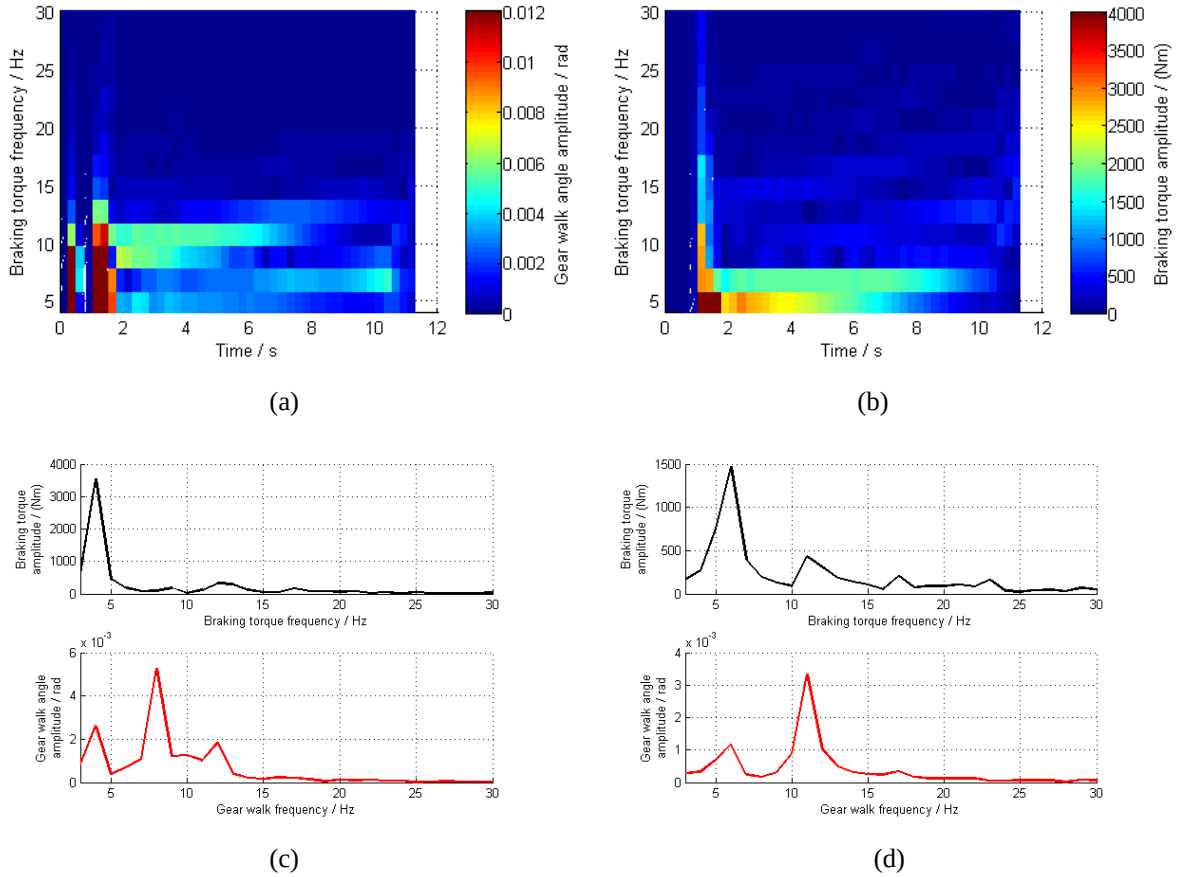

Fig. 6. Amplitude-frequency curves of gear walk response with original parameters. (a) Gear walk angle spectrogram after STFT; (b) Braking torque spectrogram after STFT; (c) Amplitude-frequency curve from 1.5s-2.5s after FFT; (d) Amplitude-frequency curve from 8s-9s after FFT.

Although Fast Fourier Transform (FFT) is not appropriate to study the dynamic system with transient response due to the fact that the frequency components are complicated and vary in the whole time domain, we can apply FFT on a short period of time to analyze the amplitude-frequency characteristics and find out the frequency relationship between the excitation braking torque and the response gear walk angle. Figures 6(c) and 6(d) are the curves obtained by FFT method in 1.5s-2.5s and in 8s-9s, respectively as the examples. In order to show clearly the dynamic components in the response, the frequency starts on the x axis from 2Hz. The black curves in the first row indicate the braking torque amplitudes in the corresponding short period, while the red curves are the gear walk angle offsets. From Figure 6(c), we can see that in 1.5s-2.5s, the main frequency of the excitation braking torque is 4Hz, and the frequency of the response gear walk is mainly composed of 4Hz, 8Hz and 12Hz, the integral multiple of the frequency of braking torque. Similarly in Figure 6(b), the braking frequency components consist of 6Hz and 11Hz, which are the same as the gear walk frequency components.

3.3 Criteria definition

In the single-objective optimizations, in order to improve the gear walk vibration performance, the maximum gear walk angle $\lambda_{\max}$ is taken as the objective function. Additional performance constraints are imposed. One of these constraints is the braking efficiency, measured using the taxiing distance. It should meet the condition

$$x_f \le x_{f0} \tag{15}$$

where x_{f0} is the taxiing distance with the original parameters, which is equal to 488.4m. Also, the rest maximum gear walk angle amplitude following the first peak A_λ, seen in Figure 5(a), is restrained by

$$A_\lambda \le \frac{1}{2} A_{\lambda \max 0}, \tag{16}$$

where $A_{\lambda \max 0}$ is the default maximum gear walk angle amplitude in the original model, which is equal to 0.023rad. Moreover, $A_{\lambda(f_\lambda \ge 10\,\mathrm{Hz})}$ and $A_{Mb(f_{Mb} \ge 10\,\mathrm{Hz})}$ representing the amplitude-frequency characteristics of the gear walk angle and the braking torque are also need to be taken into consideration. Therefore, a further two constraint conditions in this optimization problem are

$$A_{\lambda(f_\lambda \ge 10\,\mathrm{Hz})} \le \frac{1}{10} A_{\lambda \max 0}, \tag{17}$$

$$A_{Mb(f_{Mb} \ge 10\,\mathrm{Hz})} \le \frac{1}{10} A_{Mb \max 0}, \tag{18}$$

where, $A_{Mb \max 0}$ represents the default maximum amplitude of the braking torque, the value of which is 6600Nm. Eqs. (17) and (18) mean that when the gear walk vibration and the braking torque frequencies are above 10Hz, the amplitudes are ensured to be smaller than one tenth of $A_{\lambda \max 0}$ and $A_{Mb \max 0}$. Of course, for this transient brake-induced vibration, STFT is adopted to get more satisfying amplitude-frequency results with these two constraints.

Since a trade-off exists between x_f and $\lambda_{\max}$, when multi-objective optimization is considered, in addition to $\lambda_{\max}$, x_f is set as another objective function to obtain a set of non-dominated solutions and a Pareto Frontier. On account that the gear walk vibration performance and the braking efficiency are regarded as equally important objectives here, the relative weighting between these two objective functions is 1:1. By this way, the relationship between these two objective functions would be investigated. The optimization problem can be formulated as

$$\mathrm{Minimize}[x_f, \lambda_{\max}]. \tag{19}$$

with three constraints given by (16)-(18).

4 Parameter Sensitivity Study

In this section, a parameter sensitivity study is carried out to identify the most important variables for optimization in Section 5. It will be shown that the two landing gear strut parameters and the three PID control parameters play the most important role in gear walk instability and braking efficiency.

The Optimal Latin Hypercube Design (Opt LHD) method is adopted to study the parameters sensitivity of the landing gear structure and the braking control system on both the gear walk and the braking efficiency, the process of which is also called Design of Experiment (DOE) [29]. The

Opt LHD is carried out using the Computer Aided Engineering (CAE) software ISight [30] to find the parameters with greatest impact on the optimization objectives and to improve the optimization efficiency with smaller scale of the problem.

Figure 7 illustrates the DOE process using Opt LHD method to analyze the parameter sensitivity. Firstly, *m* design parameters and their value ranges should be defined. Usually the variation of these parameters would result in the change of the response. Secondly, *n* evenly distributed experimental points are generated in an *m*-dimensional space employing the Opt LHD method and a $n \times m$ matrix $\boldsymbol{X} = [\boldsymbol{X}_1, \boldsymbol{X}_2, \cdots, \boldsymbol{X}_n]^T$ is obtained. Each row of the matrix $\boldsymbol{X}$ is $\boldsymbol{X}_i^T = [x_{i1}, x_{i2}, \cdots, x_{im}] (i = 1, 2, \cdots, n)$, representing one experiment, while each column represents one parameter. Thirdly, the responses of the experiments used to measure the system performance need to be determined. After the problem definition process, the experiments should be carried out for *n* times with *n* sets of input parameters. Finally, the parameter sensitivity in terms of the variation of the design parameters could be obtained. In the DOE problem in this paper, *m* equals 9 and *n* equals 500.

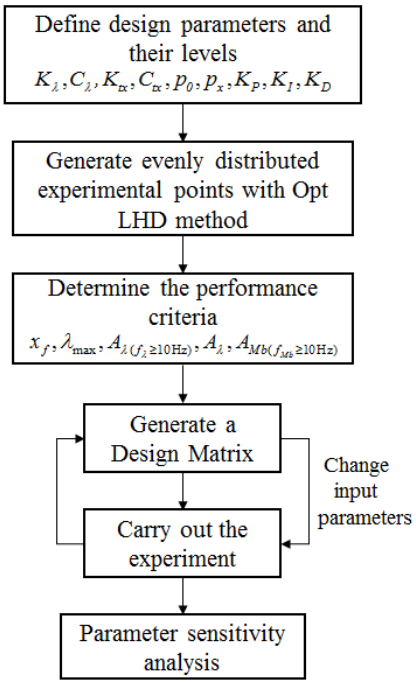

Fig. 7. A flow chart of the parameter sensitivity study process

4.1 Parameters definition

According to the gear walk mechanism and characteristics, nine key parameters of the landing gear structure and the braking control system are considered to have significant impacts on this kind of longitudinal vibration and could be changed during the landing gear design process. Three PID controller parameters K_P, K_I, K_D can be tuned in the anti-skid braking system. The braking pressure loss P_0 represents the space and wear between the braking pads and can be modified by adjusting the space and changing the braking pads. P_x indicates the hysteresis of the braking control system and can be changed by altering the braking actuators and the braking pads. The landing gear and the tire structural parameters $k_\lambda, c_\lambda, k_{tx}, c_{tx}$ can be changed by altering the structure design and the materials. However, owing to the fact that the structural parameters of all the landing

gear components need to be coordinated considering the weight, assembly, functions of landing, ground loads, steering, braking and vibration characteristics, here the value ranges of these four parameters $k_\lambda, c_\lambda, k_{tx}, c_{tx}$ are varied within ±10% based on the benchmarks.

4.2 Sensitivity analysis

As mentioned above, the DOE of the gear walk system is carried out in ISight and the sensitivity of the landing gear structural parameters and the braking control parameters are investigated. The five performance, $[x_f, \lambda_{\max}, A_\lambda, A_{\lambda(f_\lambda \geq 10\,\mathrm{Hz})}, A_{Mb(f_{Mb} \geq 10\,\mathrm{Hz})}]$, defined in Section 3 are taken as the responses in the DOE process.

Table 3

Parameter sensitivity analysis: effects on gear walk and braking response ($p_0 \in [0,2]\mathrm{MPa}$, $p_x \in [8,10]\mathrm{MPa}$, $K_P \in [10,2000]$, $K_I \in [0,3000]$, $K_D \in [0,30]$)

Design parameters	x_f	$\lambda_{\max}$	A_λ	$A_{\lambda(f_\lambda \geq 10\,\mathrm{Hz})}$	$A_{Mb(f_{Mb} \geq 10\,\mathrm{Hz})}$	Average contribution
k_λ (N/m)	16.67%	31.70%	12.28%	18.29%	2.53%	16.29%
c_λ (N·s/m)	11.10%	19.08%	19.41%	13.35%	18.62%	16.31%
k_{tx} (N/m)	8.19%	5.41%	5.15%	4.44%	4.39%	5.52%
c_{tx} (N·s/m)	5.91%	5.05%	4.40%	5.57%	3.43%	4.87%
p_0 (MPa)	7.94%	3.57%	6.19%	3.11%	6.44%	5.45%
p_x (MPa)	5.03%	2.78%	3.02%	4.05%	4.63%	3.90%
K_P	24.04%	13.63%	12.22%	12.73%	20.32%	16.59%
K_I	12.75%	12.67%	25.45%	17.44%	15.05%	16.67%
K_D	8.37%	6.11%	11.88%	21.02%	24.59%	14.39%

Table 3 demonstrates the contributions the nine key parameters made to the five performance criteria as percentage contributions. The summations of every column is 100%. Table 3 shows that the proportional coefficient K_P plays the most important role with 24.04% of the contribution to x_f. This can be explained by the fact that the value of K_P has vital influence on the output of the braking pressure. The data also indicate that the landing gear longitudinal structure parameters k_λ and c_λ affect the maximum gear walk angle $\lambda_{\max}$ greatly. The integral control coefficient K_I and the landing gear strut damping c_λ rank first and second among the contributions to A_λ. The integrator term is the error accumulation of the actual and the expected slip rates, while the damping c_λ controls the vibration attenuation. Hence they both influence the gear walk angle in the whole time domain. Further, it can be seen that K_D and k_λ account for the largest contributions to $A_{\lambda(f_\lambda \geq 10\,\mathrm{Hz})}$, as K_D has a strong impact on the high-frequency braking system and k_λ contributes to the frequency characteristic of the landing gear. In addition, three PID parameters represent more than half of the contributions on the amplitude of the high-frequency braking torque.

The far right column shows the average values of every row and it indicates that the two landing gear strut parameters k_λ, c_λ and three PID parameters K_P, K_I, K_D of the braking control system have greater effects on gear walk and braking response. Therefore, they are chosen as the variables to be designed and changed to improve the gear walk system performance in the optimization process.

5 Optimization of gear walk system

In this section, results for both the single-objective and the multi-objective optimizations will be discussed. In the single-objective optimizations part, the results of the structure and feedback control combined optimization, as well as the feedback optimization both act as bench marks. A feedforward controller is introduced and the benefit of using the feedforward controller has been shown. By using the Pareto frontier, the multi-objective optimization presents a clear trade-off between the gear walk angle and the braking efficiency.

5.1 Single-objective optimization

A global optimization method, patternsearch, is first adopted to find the minimal value of the objective function in MATLAB. Patternsearch was put forward by Hooke and Jeeves [31]. During the optimization, a direction is explored to make an improvement of the objective functions and the variables are accelerated to be optimized in this direction. Once no increase further improved the objective functions, a new direction is explored and the process is repeated until the steps are sufficiently small. This MATLAB command does not require the gradient of the problem and is effective and beneficial to the time-domain simulation. Then another local optimization method fminsearch in MATLAB is employed using the results from the patternsearch optimization as the variables' initial values for fine-tuning of the parameters in the problem. A similar approach has been successfully used in [32].

5.1.1 Structure and feedback optimization

According to the analysis in Section 4, the parameters with greatest effects on the gear walk vibration responses and braking performance are considered as the optimization variables. However, since all the materials, weight, cost, functions and vibration characteristics need to be considered during the landing gear design process, usually it is difficult to change the structure parameters. Hence in this section, the optimization considering the stiffness and damping coefficient of the landing gear strut k_λ, c_λ together with K_P, K_I, K_D of the PID controller is only used as a benchmark for comparison.

Table 4 shows the optimization results. It can be seen that the taxiing distance is far lower than the constraint value and the maximum gear walk angle decreases by 10.81%. In this optimization problem, the optimization objective is only to minimize the maximum gear walk angle, while the taxiing distance is regarded as the constraint that only need to be restricted within a certain value rather than to be the minimum. Therefore, comparing to the original parameters in Table 1, the landing gear strut stiffness k_λ and damping c_λ with significant influence on the maximum gear walk angle $\lambda_{\max}$ both reach the maximum values to obtain the smallest vibration angle. Furthermore, the three PID control parameters are also changed a lot. The values of K_P and K_D both increase about 5 times. This can be interpreted by the fact that K_P has significant impact on the taxiing distance, while K_D affects high-frequency amplitudes greatly.

Table 4

Optimization result and corresponding parameter values*

Performance	Optimal parameter values

Variables	x_f (m)	$\lambda_{\max}$ (rad)	K_P	K_I	K_D	k_λ (N/ m)	c_λ (N·s/m)
Optimization values and improvements	457.5	0.066 (10.81%)	544	2880	5	1920600	15180

*% improvements are given in bracket for the criteria being optimized, similarly in Tables 4 and 5.

5.1.2 Feedback optimization

In this optimization problem, k_λ, c_λ stay unchanged and the variables are only three PID control parameters.

Table 5 presents the optimization results of the three PID control variables and the system responses. Comparing to the original model, the taxiing distance decreases to 456.9m, indicating that the optimization with these three PID control parameters would improve the braking efficiency effectively. In addition, in comparison with the parameter values of K_P, K_I, K_D, K_P remains unchanged, while K_I and K_D both altered by approximately 20%. Although these three values do not change too much, the resulting taxiing distance is shorter than the result in Section 5.1, revealing that while an increase in k_λ, c_λ will reduce the gear walk angle, the braking efficiency will be decreased slightly. Table 5 shows that the maximum gear walk angle only decreases by 1.35% compared to the original model. Despite of this, Table 2 illustrates K_P and K_I has great effects on $\lambda_{\max}$, the value of $\lambda_{\max}$ still changes little after the optimization in that four constraints exist to restrict the ranges of the parameters variation.

Table 5

Optimization result and corresponding parameter values

Variables	Performance		Optimal parameter values		
	x_f (m)	$\lambda_{\max}$ (rad)	K_P	K_I	K_D
Optimization value and improvements	456.9	0.073(1.35%)	544	2236	6

5.1.3 Feedforward and feedback optimization

From Section 5.1.1 and 5.1.2, we find that after the optimizations, the overshoots of the gear walk angle and the braking torque are still very high at the beginning of the braking process. For the purpose of eliminating these significant overshoots, a first-order feedforward transfer function is added to the braking control system to modify the expected value such that the slip rate increases from 0 to the optimal slip rate σ_m gradually rather than as a sudden step rise. The new expected slip rate σ_b is given by

$$\sigma_b = \begin{cases} 0 & 0 \le t < 1 \\ \sigma_{\mathrm{m}} \cdot \dfrac{b}{s+b} & t \ge 1 \end{cases} \qquad b \in [2,1000], \tag{20}$$

where b is inversely proportional to the settling time of the function, indicating the rate of increase of the expected slip rate. As a result, in this section, the optimization variables are the three PID control parameters K_P, K_I, K_D and the new parameter b.

From Table 6, we can see the optimization results of the four parameter values and that the maximum gear walk angle decreases remarkably by 25.68% compared to the original results, even twice larger than the improvement of increasing the landing gear strut stiffness and damping by

10%. The value of K_P increases greatly to shorten the taxiing distance x_f under the settled value. Although the x_f meets the constraint, the result almost approaches the constraint value x_{f0}, which means the variation of *b* has a significant impact on the braking efficiency and the crest of the gear walk angle.

Table 6

Optimization result and corresponding parameter values

Variables	Performance		Optimal parameter values			
	x_f (m)	$\lambda_{\max}$ (rad)	K_P	K_I	K_D	b
Optimization values and improvements	488.3	0.055(25.68%)	1056	2117	6	64

5.1.4 Comparison and analysis of results

Figure 8 shows the simulation results of the gear walk and braking responses for the three single-objective optimizations presented above. Figure 8(a) reveals that the actual slip rate curves all remain near the optimal value with slight vibration almost during the whole braking process except for the initial moment at 1s when the braking system starts to work. Comparing with Figure 4, the large fluctuation of the slip rate curve has disappeared, but there still exists overshoots in the structure and feedback optimization and feedback optimization, while in the feedforward optimization, the slip rate rises slowly from 1s to 2.5s without the big overshoot so that during this period, the braking efficiency is lower but the overshoots of the gear walk angle and the braking torque are both smaller. Figures 8(b) and 8(c) illustrate that the gear walk responses are similar to the braking torque excitations. Not only does the peak value of the gear walk angles decrease, but the vibrations also decay faster and tends to a stable value by about 2.5s. Although the balance values of the braking torques are the same for the three optimizations, in the structure and feedback optimization, the balance value of the gear walk angle is small than the other two conditions in that the landing gear strut stiffness is larger than those of the others. Apart from the maximum gear walk angle amplitudes, all the other amplitudes are smaller than 0.004rad. When the frequency is high, the gear walk angle amplitudes are all smaller than 5×10^{-4} rad and the braking torque amplitudes are smaller than 400 N·m. Therefore, they satisfy the other three constraints in the optimization problem.

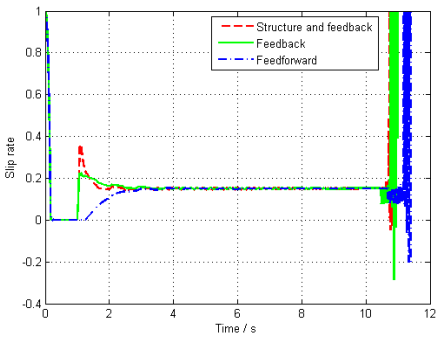

(a)

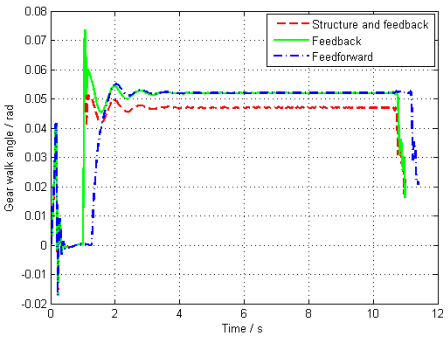

(b)

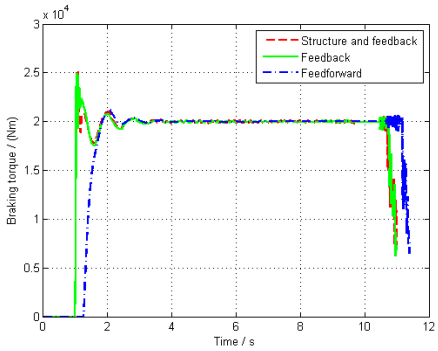

Fig. 8. Simulation results of three single-objective optimizations. (a) Slip rate; (b) Gear walk angle; (c) Braking torque.

5.1.5 Stability and robustness of optimized control system

From the three optimized results in Figure 8, it can be seen that after adding feedforward control in the braking system, the maximum gear walk angle reduces more than 25% while the landing gear structure parameters remained the same and the braking efficiency is ensured. Therefore, different working conditions under the optimized control parameters of the feedforward and feedback optimization are simulated to ensure the stability and robustness of the optimized control system.

(1) Runway surface

Different weathers may result in wet or icy runway surfaces, which will make the frictional coefficient between the ground and the main tire decreases according to Eq. (11). Keeping other working conditions unchanged, Figure 9 demonstrates the gear walk and braking simulation results of the optimized control system on different runway surfaces.

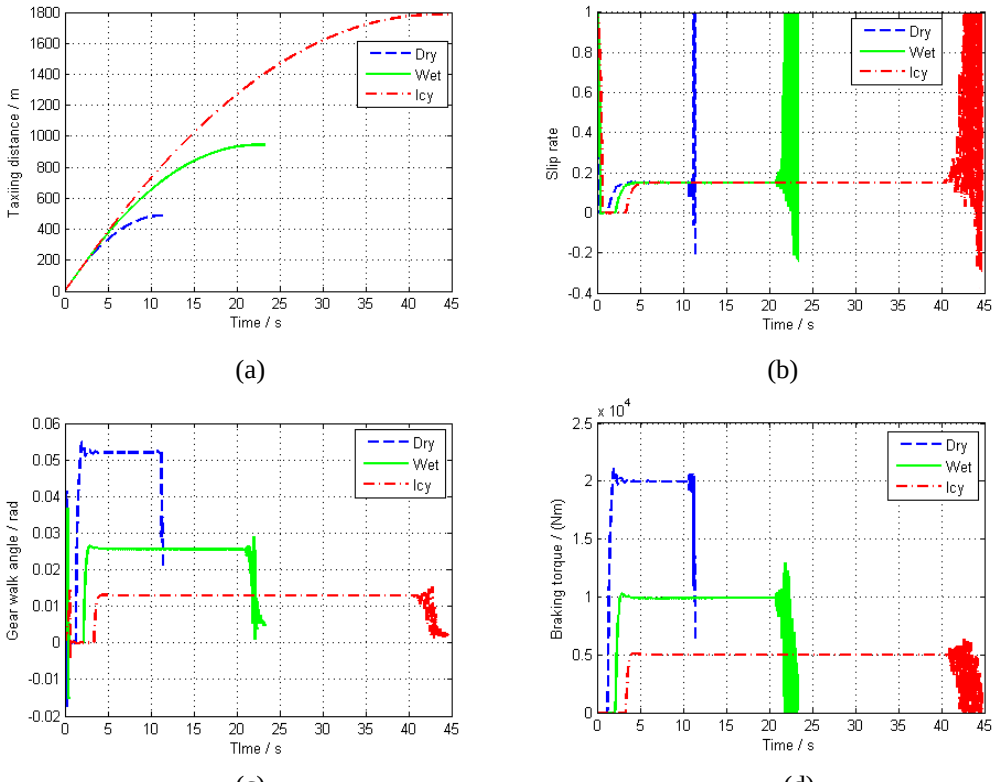

Fig. 9. Simulation results on different runway surfaces. (a) Taxiing distance; (b) slip rate; (c) gear walk

angle; (d) braking torque.

Figure 9 reveals that as the frictional coefficient decrease, it takes longer time for the slip rate to reach the respect value and the taxiing distance also becomes longer. Smaller friction force leads to smaller braking torque, so that the gear walk vibration tends to be gentle and even the overshoots of the braking torque and the gear walk angle disappear. However, see Figures 9(b), 9(c) and 9(d), due to the poor performance of the PID braking control law during the aircraft low-speed rollout period, the slip rate and the gear walk angle fluctuate greatly at the last 3 seconds of the braking process, serious skidding exists in the braking wheel and as the runway surface condition gets worse, the skidding phenomenon becomes severer.

(2) Landing gear initial sink speed

The landing gear initial sink speed is one of the most important parameters during the landing phase. It has great impact on shock absorber stroke, the influence of which on gear walk is considered in this paper. Thus, Figure 10 illustrates the gear walk and braking responses under different sink speeds of 0.5m/s, 1m/s and 2m/s.

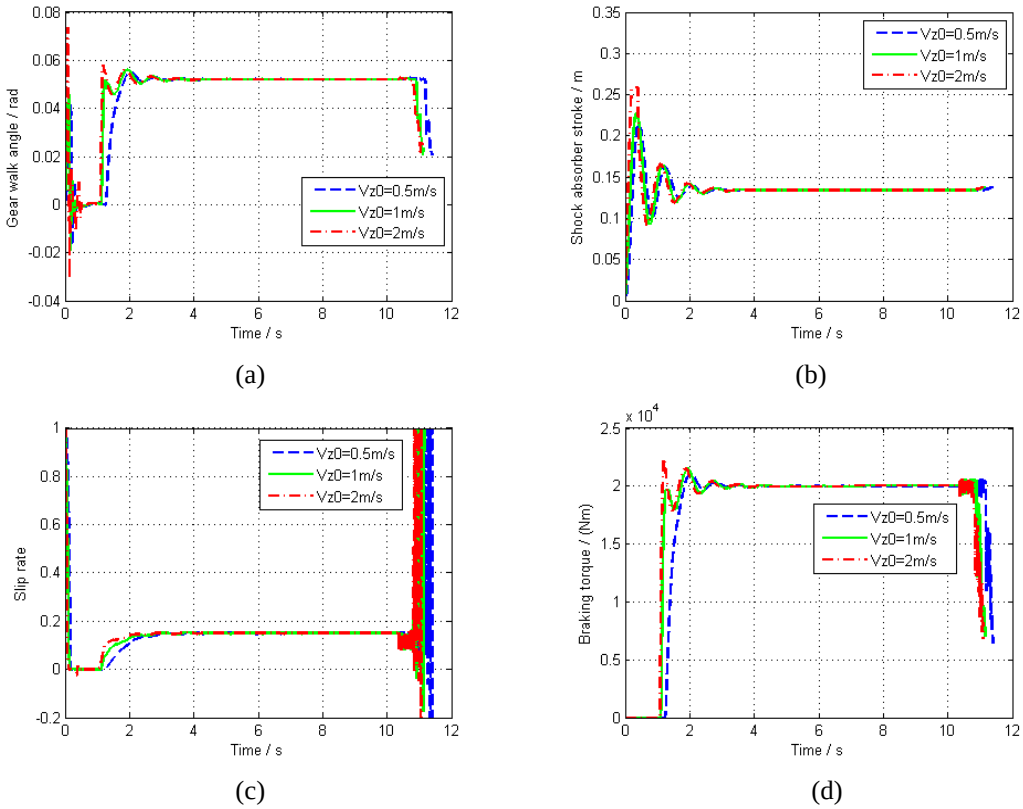

Fig. 10. Simulation results of different sink speeds. (a) Gear walk angle; (b) Shock absorber stroke; (c) slip rate; (d) braking torque.

From Figure 10, we can see that larger sink speed results in larger stroke and as well larger rate of stroke change. As a result, the slip rate increases to the optimal value faster. In addition, as the sink speed rises, the maximum values and the overshoots of braking torque and gear walk angle increase a little. The braking time is shortened slightly. Simulation results in this section indicate that this optimized the braking control system is of good stability and robustness under different

working conditions.

5.2 Multi-objective optimization

In practical engineering projects, there mostly exist multi-objective optimization problems. Interaction among various objectives should be carefully considered since the improvement of one objective would sacrifice another objective performance. Generally, it is impossible to obtain an optimal solution satisfying every single requirement. Based on Multi-Objective Genetic Algorithm (MOGA) method, we can obtain a set of non-dominated solutions, denoted as Pareto Frontier in the objective functions space.

Definition 1 (Dominance [33]*): J(μ') dominates J(μ'') if for all objectives, J(μ') is not worse than J(μ''), that is, $J_i(\mu') \leq J_i(\mu'')$, i=1,2,…,m and $J_i(\mu') < J_i(\mu'')$ for at least i, $1 \leq i \leq m$.*

Definition 2 (Pareto optimality [33]*): J(μ') is a Pareto optimal solution if there is no other objective vector J(μ'') such that $J_i(\mu'') \leq J_i(\mu')$ for all i=1,2,…,m and $J_i(\mu') < J_i(\mu'')$ for at least i, $1 \leq i \leq m$.*

Definition 3 (Non-dominated set [34]*): J(μ') is non-dominated if there is no J(μ'') that dominates J(μ'). The set of all non-dominated points is called the non-dominated set.*

where, μ' and μ'' are the solutions in the solution set space, m is the number of cost functions, J_i represents the cost functions.

Figure 11 demonstrates the flow chart of MOP in three stages. First step is the problem definition including the optimization variables, the objective functions and the constraints conditions. Secondly, the MOP is carried out by an MOGA method and the last stage is to make a decision to select a single solution, which is the best compromise according to other requirements in the landing gear design process.

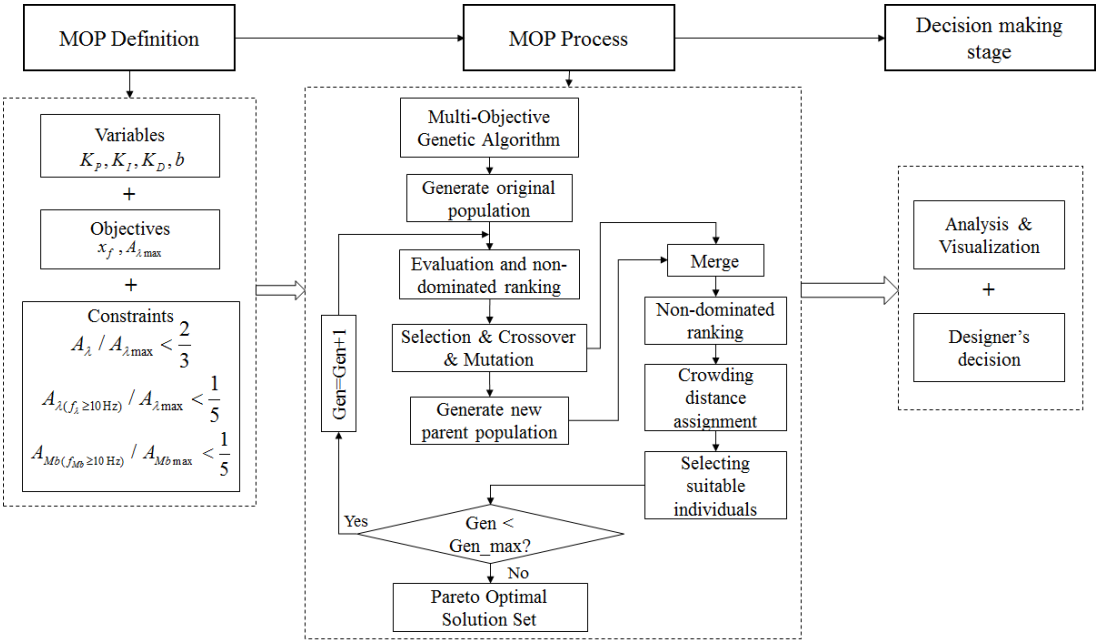

Fig. 11. Flow chart of MOP using Multi-Objective Genetic Algorithm

Since the landing gear structure parameters are difficult to change and the maximum gear walk angle amplitude decreases a lot after adding the new parameter *b*, the optimization variables in the

MOP are the PID parameters K_P, K_I, K_D and the parameter *b* in the first-order transfer function, the same as those in Section 5.1.3.

The multi-objective optimization is conducted in MATLAB using the controlled elitist genetic algorithm (a variant of Non-dominated Sorting Genetic Algorithm II). The elitist strategy is introduced to guarantee that some excellent individuals will not be abandoned in the evolution process, and then the non-dominated ranking will merge the parent population with the progeny population, ensuring that the next population can be selected from the doubled space with a proportion of the elitist individuals retained. The method is also characterized as high efficiency and good convergence of the solution set. The command of the multi-objective genetic algorithm in MATLAB is gamultiobj and the initial value ranges are located near the optimal values obtained in Section 5.1.3. In addition, the population size is 80 and the evolutional generation is 200. Also the Pareto fraction representing the percentage of individuals in the current population on the Pareto front is set to 0.5.

Figure 12 shows the Pareto Frontier of the two objectives $\lambda_{\max}$ and x_f. Nine non-dominated solutions are obtained after the multi-objective optimization and each point in the Pareto Frontier respectively corresponds to a Pareto optimal solution. As the maximum gear walk angle decreases, the taxiing distance becomes longer. The frontier represents a boundary, revealing that no better solutions would be situated in the bottom-left region of the frontier.

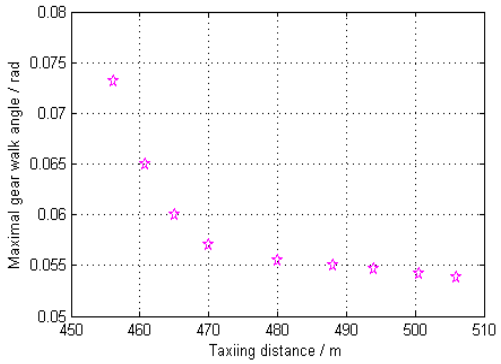

Fig. 12. Pareto frontier of multi-objective optimization

Table 7 gives the specific values of the Pareto solution set and the Pareto Frontier as well as their comparisons to the original results. From columns 4, 5 and 6 of Table 7, it can be seen that the reduction of the value *b* leads to the decrease of both the peak vibration angle and the braking efficiency. The percentage changes of $\lambda_{\max}$ and x_f relative to their original results are given in brackets.

Table 7

Pareto solution set and optimization results comparison

K_P	K_I	K_D	b	$\lambda_{\max}$ (rad) and improvements	x_f (m) and improvements
529	2078	6	675	0.0732 (1.08%)	456.1 (6.61%)
886	1914	6	202	0.0653 (11.76%)	460.7 (5.67%)
478	2750	5.5	145	0.0618 (16.49%)	465.1 (4.77%)

531	872	8.7	114	0.0566 (23.51%)	469.8 (3.77%)
799	1513	7	81	0.0559 (24.46%)	480.4 (1.64%)
1085	2117	6	49	0.0550 (25.68%)	488.0 (0.08%)
853	1177	8	39	0.0546 (26.22%)	494.0 (-1.15%)
948	2456	5	28	0.0542 (26.76%)	500.5 (-2.48%)
912	2530	7	17	0.0539 (27.16%)	506.3 (-3.67%)

The last stage of MOP is decision-making, the ultimate goal of which is to choose a single solution in accordance with the designer's preferences including the runway length restriction, the landing condition, the landing gear structural strength and the fatigue life of the landing gear components.

6 Conclusion

A nonlinear dynamic gear walk model was established with the coupling of the shock absorber stroke and the longitudinal motion being considered. The influence of the parameters on both the gear walk vibration and the braking efficiency has been studied. Single-objective and multi-objective optimizations using proposed performance criteria and constraints have been carried out. The conclusions are drawn as below:

(1) Through parameter sensitivity study, it has been found that the two landing gear strut parameters k_λ, c_λ and three PID parameters K_P, K_I, K_D of the braking control system have greater effects on gear walk and braking response. These five variables all account for about 15% of the contribution respectively, while other parameters only occupy about 5%;

(2) The Short Time Fourier Transform method has been found to be useful for characterizing the gear walk transient amplitude-frequency properties and the gear walk frequency components are integral multiple of braking frequency components;

(3) When both the landing gear structure and the braking control parameters are optimized, a 10.81% improvement of the maximum gear walk angle is obtained; while if k_λ, c_λ are fixed, the peak value of gear walk will only be improved by 1.35%;

(4) A feedforward control is proposed as part of the braking control. Optimizing the PID parameters and the variable *b* effectively reduces the maximum peak gear walk angle by 25.68%, while keeping the taxiing distance within constraints. The robustness of this control law is verified;

(5) Multi-objective optimizations using the PID and feedforward parameters have been carried out. A boundary revealing that no better solutions would be situated in the bottom-left region of the Pareto frontier has been obtained. The result demonstrates the trade-off between the gear walk vibration and the braking efficiency.

Conflict of interest statement

The authors declare no conflict of interest.

Acknowledgements

This study was funded by the National Natural Science Foundation of China (Grant No.11372129), the National Defense Outstanding Youth Science Foundation (Grant No.2018-JCJQ-ZQ-053), the China Postdoctoral Science Foundation Funded Project (Grant No.2019M650115), Jiangsu Planned Projects for Postdoctoral Research Funds, the Research Fund of State Key Laboratory of Mechanics and Control of Mechanical Structures (Nanjing University of Aeronautics and astronautics) (Grant No.MCMS-0217G01), the Fundamental Research Funds for the Central Universities (Grant No.NP2017401), the Priority Academic Program Development of Jiangsu Higher Education Institutions, Specialized Research Fund for the Doctoral Program of Higher Education(Grant No. 20123218120003).

Appendix A.

The gear walk dynamic model is established using the Lagrange's equation

$$\frac{\partial}{\partial t}\frac{\partial L}{\partial \dot{q}_i}-\frac{\partial L}{\partial q_i}+\frac{\partial R}{\partial \dot{q}_i}=Q_i, \tag{A.1}$$

where R is the dissipation of energy, q_i and Q_i represent the generalized independent coordinates and generalized forces, respectively, and $L=T-V$. T is the kinetic energy of the system and V is the potential energy of the system.

The total kinetic energy T of the gear walk system is

$$\begin{aligned} T=&\frac{1}{2}M(\dot{x}_f^2+\dot{z}_f^2)+\frac{1}{2}m_1(\dot{x}_1^2+\dot{z}_1^2)+\frac{1}{2}(J_1+m_1 l_0{}^2)\dot{\lambda}^2+\frac{1}{2}m_2(\dot{x}_2^2+\dot{z}_2^2)\\ &+\frac{1}{2}(J_2+m_2(l_0+l_1-s+l_2/2)^2)\dot{\lambda}^2+\frac{1}{2}m_w(\dot{x}_w^2+\dot{z}_w^2)\\ &+\frac{1}{2}(J_{wt}+m_w(l_0+l_1-s+l_2)^2)\dot{\lambda}^2+\frac{1}{2}J_w\dot{\theta}_w^2+\frac{1}{2}J_t\dot{\theta}_t^2. \end{aligned} \tag{A.2}$$

Elastic potential energy stored by four springs representing the landing gear longitudinal stiffness k_λ, the tire vertical stiffness k_t, the tire longitudinal stiffness k_{tx} and the shock absorber stiffness k_s. Thus, the potential energy V of the system is described as

$$V=-Mg\cdot z_f-m_1 g\cdot z_1-m_2 g\cdot z_2-m_w g\cdot z_w+\frac{1}{2}k_\lambda\lambda^2+\frac{1}{2}k_s s^2+\frac{1}{2}k_t\delta_t^2+\frac{1}{2}k_{tx}R_h^2(\theta_w-\theta_t)^2. \tag{A.3}$$

The energy dissipation term consists of the damping of the landing gear strut, the shock absorber and the tire longitudinal characteristics. It is given by

$$R=\frac{1}{2}c_\lambda\dot{\lambda}^2+\frac{1}{2}c_s\dot{s}^2+\frac{1}{2}c_{tx}R_h{}^2(\dot{\theta}_w-\dot{\theta}_t)^2. \tag{A.4}$$

The generalized forces are defined as

$$Q_i=\frac{\delta A}{\delta q_i}, \tag{A.5}$$

where δA is the virtual work done to the gear walk model, and is given by

$$\delta A=f(-\delta x_w+\delta\theta_t\cdot R_g)-M_b\cdot\delta\theta_t. \tag{A.6}$$

Here f is the friction force between the ground and the tire, δx_w is the virtual displacement of the wheel center, $\delta\theta_t$ is the virtual rotational angle of the braking tire.

The top of the strut is attached to the fuselage, so the movement of the outer cylinder mass center x_1, z_1 is related to the fuselage movement x_f, z_f and gear walk angle λ, giving

$$x_1=x_f-l_0\cdot\sin\lambda, \tag{A.7}$$

$$z_1 = z_f + l_0 \cdot \cos\lambda. \tag{A.8}$$

Since the relative movement of the outer cylinder and the piston rod is the shock absorber stroke *s*, the displacement of the piston rod mass center x_2, z_2 is

$$x_2 = x_f - (l_0 + l_1 - s + \frac{l_2}{2})\sin\lambda, \tag{A.9}$$

$$z_2 = z_f + (l_0 + l_1 - s + \frac{l_2}{2})\cos\lambda. \tag{A.10}$$

The braking wheel center is fixed on the bottom of the piston rod through a wheel axle, so the motion of the braking wheel center x_w, z_w can be expressed as

$$x_w = x_f - (l_0 + l_1 - s + l_2)\sin\lambda, \tag{A.11}$$

$$z_w = z_f + (l_0 + l_1 - s + l_2)\cos\lambda. \tag{A.12}$$

Appendix B.

Table B.1

Parameters and their values used in the gear walk model

Parameter	Value (default)
Geometry parameters	
Distance between strut top and outer cylinder mass center, l_0	0.68 m
Initial distance between piston rod top and outer cylinder mass center, l_1	0.33 m
Piston rod length, l_2	0.67 m
Structure parameters	
Equivalent mass of fuselage, *M*	7020.7 kg
Mass of outer cylinder, m_1	118.4 kg
Mass of piston rod, m_2	58.1 kg
Stiffness of shock absorber, k_s	5.1×10^5 N/m
Damping of shock absorber, c_s	2.9×10^4 N s/m
Tire parameters	
Original radius of main wheel, R_w	0.38 m
Radius of main wheel hub, R_h	0.18 m
Mass of main wheel, m_w	104.7 kg
Moment of inertia of main wheel hub about wheel center, J_w	1.15 kg m^2
Moment of inertia of main tire about wheel center, J_t	3.07 kg m^2
Vertical stiffness of main wheel, k_t	2.5×10^6 N/m

Reference

[1] J. Pritchard, Overview of Landing Gear Dynamics Introduction, J. Aircr. 38 (2001) 130–137. doi:10.2514/2.2744.

[2] O. Hamzeh, W. Tworzydlo, H. Chang, S. Fryska, Analysis of friction-induced instabilities in a simplified aircraft brake, SAE Trans. 108 (2000) 3404–3418. doi:10.4271/1999-01-3404.

[3] J.J. Sinou, O. Dereure, G.B. Mazet, F. Thouverez, L. Jezequel, Friction-induced vibration for an aircraft brake system - Part 1: Experimental approach and stability analysis, Int. J. Mech. Sci. 48 (2006) 536–554. doi:10.1016/j.ijmecsci.2005.12.002.

[4] Y. Ku, Interaction between braking and landing gear vibration, Acta Aeronaut. Astronaut. Sin. 18 (1996) 228–230.

[5] L. Zhang, D. Zhu, On the dynamic properties of landing gear walking, Acta Aeronaut. Astronaut. Sin. 17 (1996) 292–296.

[6] B. Karthik, F. Kambiz, Gear walk instability studies using a vibration model of a reduced scale landing gear system, in: Proc. DETC'02 ASME 2002 Des. Eng. Tech. Conf. Comput. Inf. Eng. Conf., Montreal,Canada, 2002: pp. 243–251.

[7] P.D. Khapane, Gear walk instability studies using flexible multibody dynamics simulation methods in SIMPACK, Aerosp. Sci. Technol. 10 (2006) 19–25. doi:10.1016/j.ast.2005.07.009.

[8] R. Lernbeiss, M. Plochl, Simulation model of an aircraft landing gear considering elastic properties of the shock absorber, Proc. Inst. Mech. Eng. Part K-Journal Multi-Body Dyn. 221 (2007) 77–86. doi:10.1243/1464419jmbd63.

[9] S. Gualdi, M. Morandini, G.L. Ghiringhelli, Anti-skid induced aircraft landing gear instability, Aerosp. Sci. Technol. 12 (2008) 627–637. doi:10.1016/j.ast.2008.02.002.

[10] P.D. Khapane, Simulation of Landing Gear Dynamics Using Flexible Multi-Body Methods, in: 25th Int. Congr. Aeronaut. Sci., Hamburg,Germany, 2006: pp. 3–8.

[11] F. Zhang, M. Wei, Multi-objective optimization of the control strategy of electric vehicle electro-hydraulic composite braking system with genetic algorithm, Adv. Mech. Eng. 7 (2015) 1–8. doi:10.1177/1687814014568491.

[12] J. Velasco-Carrau, S. Garc á-Nieto, J. V. Salcedo, R.H. Bishop, Multi-Objective Optimization for Wind Estimation and Aircraft Model Identification, J. Guid. Control. Dyn. 39 (2016) 372–389. doi:10.2514/1.G001294.

[13] X.H. Wei, Q.Z. Yin, H. Nie, M. Zhang, Z.L. Tao, Aircraft electric anti-skid braking system based on fuzzy-PID controller with parameter self-adjustment feature, Trans. Nanjing Univ. Aeronaut. Astronaut. 31 (2014) 111–118.

[14] B. Wang, X.Y. Huang, J.M. Wang, X.X. Guo, X.Y. Zhu, A robust wheel slip ratio control design combining hydraulic and regenerative braking systems for in-wheel-motors-driven electric Vehicles, J. Franklin Inst. 352 (2015) 577–602. doi:10.1016/j.jfranklin.2014.06.004.

[15] Y.R. Li, Z.H. Zhang, J.L. Xu, Study on Fuzzy Sliding-Mode Variable Structure Control for Aircraft Anti-skid Braking, J. Northwest. Polytech. Univ. 33 (2015) 45–49.

[16] W. Kruger, I. Besselink, D. Cowling, D.B. Doan, W. Kortum, W. Krabacher, Aircraft landing gear dynamics: simulation and control, Veh. Syst. Dyn. 28 (1997) 119–158. doi:10.1080/00423119708969352.

[17] N. Novakovic, One Approach to the Aircraft Brake Control System Numeric Identification Method, SAE Int. J. Commer. Veh. 8 (2015) 302–309. doi:10.4271/2015-01-2693.

[18] S.M. Savaresi, M. Tanelli, C. Cantoni, Mixed Slip-Deceleration Control in Automotive

Braking Systems, J. Dyn. Syst. Meas. Control. 129 (2007) 20–31. doi:10.1115/1.2397149.
[19] V. Pilipchuk, P. Olejnik, J. Awrejcewicz, Transient friction-induced vibrations in a 2-DOF model of brakes, J. Sound Vib. 344 (2015) 297–312. doi:10.1016/j.jsv.2015.01.028.
[20] J.-S. Park, Optimal Latin-hypercube designs for computer experiments, J. Stat. Plan. Inference. 39 (1994) 95–111. doi:10.1016/0378-3758(94)90115-5.
[21] E. Zitzler, L. Thiele, Multiobjective evolutionary algorithms: a comparative case study and the strength Pareto approach, IEEE Trans. Evol. Comput. 3 (1999) 257–271. doi:10.1109/4235.797969.
[22] S.A. Batterson, A study of the dynamics of airplane braking systems as affected by tire elasticity and brake response, NASA Langley Research Center,Hampton, VA, United States, NASA-TN-D-3081, 1965.
[23] R. Van Der Valk, H.B. Pacejka, An Analysis of a Civil Aircraft Main Gear Shimmy Failure, Veh. Syst. Dyn. 22 (1993) 97–121. doi:10.1080/00423119308969023.
[24] K. Ro, A descriptive modeling and simulation of aircraft-runway dynamics, in: 44th AIAA/ASME/ASCE/AHS/ASC Struct. Struct. Dyn. Mater. Conf., American Institute of Aeronautics and Astronautics, Inc, Norfolk,Virginia, 2003. doi:10.2514/6.2003-1895.
[25] H. Bin Song, B. Fang, P. Wang, Research and applications of immune PID adaptive controller in anti-skid braking system for aircraft, in: Int. Conf. Inf. Eng. Comput. Sci. ICIECS 2009, 2009: pp. 1–5. doi:10.1109/ICIECS.2009.5363257.
[26] J. Sen Wang, C.A. He, Determination of tire-runway friction coefficient, J. Northwest. Polytech. Univ. 18 (2000) 569–571.
[27] M. Zhang, Research on some key technologies of aircraft ground dynamics, Nanjing University of Aeronautics and Astronautics, 2009.
[28] Q.Z. Yin, H. Nie, M. Zhang, Y.Q. Wang, J. Deng, Analysis of the influence of braking control laws on gear walk, J. Vibroengineering. 18 (2016) 1723–1741. doi:http://dx.doi.org/10.21595/jve.2016.16391.
[29] R. Jin, W. Chen, A. Sudjianto, An efficient algorithm for constructing optimal design of computer experiments, J. Stat. Plan. Inference. 134 (2005) 268–287. doi:10.1016/j.jspi.2004.02.014.
[30] S.L. Padula, J.J. Korte, H.J. Dunn, A.O. Salas, Multidisciplinary Optimization Branch Experience Using iSIGHT Software, NASA Langley Research Center; Hampton, VA United States,NASA/TM-1999-209714, 1999.
[31] R. Hooke, T.A. Jeeves, “Direct Search” Solution of Numerical and Statistical Problems, J. Assoc. Comput. Mach. 8 (1961) 212–229. doi:10.1145/321062.321069.
[32] J.Z. Jiang, A.Z. Matamoros-Sanchez, A. Zolotas, R.M. Goodall, M.C. Smith, Passive suspensions for ride quality improvement of two-axle railway vehicles, Proc. Inst. Mech. Eng. Part F J. Rail Rapid Transit. 229 (2013) 315–329. doi:10.1177/0954409713511592.
[33] K. Miettinen, “Concepts,” Nonlinear MultiObjective Optimization, Springer Science & Business Media, 1999.
[34] M.P. Hansen, A. Jaszkiewicz, Evaluating the quality of approximations to the non-dominated set, Institute of Mathematical Modelling,Technical Universityof Denmark,IMM Technical Report IMM-REP-1998-7, 1998.